

Intrinsic interface states in InAs-AlSb heterostructures

F. Raouafi,¹ R. Benchamekh,^{2,3} M.O. Nestoklon,^{2,4} J-M. Jancu,⁵ and P. Voisin²

¹*Laboratoire de Physico-chimie des Microstructures et Micro-systèmes, Institut*

Préparatoire aux Etudes Scientifiques et Techniques, BP51, 2070 La Marsa, Tunisia

²*CNRS-Laboratoire de Photonique et de Nanostructures, route de Nozay, F-91460, Marcoussis, France*

³*Tyndall National Institute, Lee Maltings, Dyke Parade, Cork, Ireland*

⁴*Ioffe Physical-Technical Institute of the Russian Academy of Sciences, St. Petersburg 194021, Russia*

⁵*FOTON, Université Européenne de Bretagne, INSA-Rennes and CNRS, Rennes, France*

(Dated: April 27, 2015)

We examine the formation of intrinsic interface states bound to the plane of In-Sb chemical bonds at InAs/AlSb interfaces. Careful parameterization of the bulk materials in the frame of the extended basis *spds** tight-binding model and recent progress in predictions of band offsets severely limit the span of tight-binding parameters describing this system. We find that a heavy-hole like interface state bound to the plane of In-Sb bonds exists for a large range of values of the InSb/InAs band offset.

I. INTRODUCTION

Ever since the seminal papers of I.Tamm¹, the possible existence of intrinsic surface or interface states in semiconductors has been a hotly debated issue, but the emerging topic of topological insulators has recently renewed the interest in this field², in connection with predicted “quantum immunity” of edge-state currents against scattering. In the early 80’s, a first type of interface state was predicted to occur in HgTe/CdTe heterostructures^{3–5}, due to the boundary conditions between the inverted band structure of HgTe and the normal band structure of CdTe.

In that case, existence of interface states is primarily due to anomalous properties of one of the bulk constituents. Much more recently, the attention was drawn to the original situation of interfaces between materials sharing no common atom (NCA), like InAs/GaSb, InAs/AlSb, BeTe/ZnSe or (InGa)As-InP. In these materials, interfaces involve chemical bonds that do not exist in the host materials, for instance In-Sb or Ga-As in the first example. Such interface bonds can in principle act as a local potential well that may capture the carriers. This second type of interface state, if it exists, relies mainly on local interface properties and proper modeling requires detailed atomic-scale information that is normally missed by the standard envelope-function approximation^{6,7}. The existence of interface states in the InAs/AlSb system was first suggested heuristically by Kroemer et al. in 1992⁸ as a possible explanation for the heavy n-type doping observed in nominally undoped superlattices, but it was soon argued that possible values of band offsets would not allow for an interface state resonant with conduction band⁹. Later, this question was revisited using ab initio methods by Shaw et al.^{10,11}, who concluded to localization of the hole ground state near the plane of In-Sb bonds. However, in the bare DFT without spin-orbit interaction used in these calculations, InAs and InSb are metals rather than semiconductors¹², and this makes comparison to experimental results difficult. InAs/AlSb has a type II

band line-up with ground electrons (holes) in the InAs (AlSb) layers, and reported values of valence band offset in the 100-200 meV range^{13,14}. In recent years, the InAs/AlSb system has proved its technological importance with the emergence of high performance optoelectronic devices based on intersubband transitions, such as quantum cascade lasers¹⁵ in the mid-infrared. A need to better analyze and control interface composition was evidenced¹⁶, as large strain can accumulate and lead to plastic relaxation when preferential formation of Al-As interface bonds prevails. Besides recent progress in electron microscopy that allow for chemical and strain analysis with sub-nanometer resolution^{16,17}, it has become possible to observe directly the wavefunctions of quantum states using STM¹⁸. Thus, advances in fine material characterization offer a unique opportunity to get conclusive experimental proofs on the existence of intrinsic interface states. On the modeling side, progress in computing would now allow for ab-initio studies combining full atomic relaxation and realistic electronic structure of narrow gap semiconductors, but there is also room for computationally easier, yet predictive calculations based on empirical-parameter atomistic theories such as advanced empirical tight-binding (ETB)¹⁹ or atomistic empirical pseudo-potentials (AEPP)^{20,21} schemes. A *sp*³ ETB model with first and second neighbor interactions was first used by Theodorou et al.²². Late, modeling of InAs/AlSb and ZnSe/BeTe within the *sp*3s* tight binding model was discussed by Nestoklon et al.²³. In this early work, besides the intrinsic limitation of the *sp*3s* model for precision modeling, effects of large strain of interface bonds were not discussed, and simply “renormalized” in the interfacial s-p two-center integrals considered as adjustable parameters. Proper consideration and full modeling of elastic relaxation actually reduces the number of adjustable parameters to few band offset parameters. The purpose of this paper is to re-examine the particular case of InAs-AlSb quantum wells using an advanced tight-binding scheme, integrating recent methodological progress in the treatment of strain, and delineate the range of parameters for which intrinsic interface

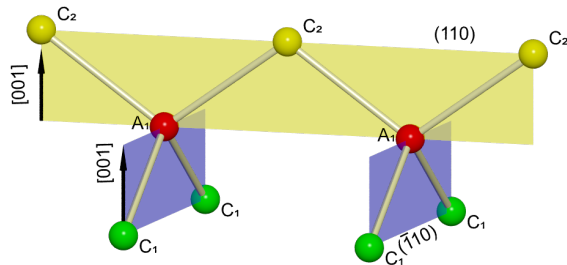


FIG. 1. sketch of the arrangement of chemical bonds at a C_1A_1/C_2A_2 interface grown along the $[001]$ direction. C and A stand for Cation and Anion species, respectively.

states would exist in this system.

In the case of standard $[001]$ growth axis, the mere presence of an interface between materials C_1A_1 and C_2A_2 (where A and C stand for anion and cation species) breaks not only the translational invariance but also a rotational degree of freedom, as the four-fold roto-inversion (or S_4) symmetry of the T_d point group is no longer allowed. The atomic arrangement in the interface cell is shown in Fig. 1 and illustrates that at the interface the C_1A_1 bonds lie in the $(\bar{1}10)$ plane while the A_1C_2 bonds lie in the (110) plane.

The corresponding point group symmetry is C_{2v} . For a symmetric quantum well with equivalent interfaces, a S_4 symmetry operation centered on an atom in the central layer exists and transforms one interface into the other, upgrading overall symmetry to D_{2d} . Although these features were clearly stated in early publications on tight-binding calculations^{24–27}, it is only in the mid 90s that the resulting consequences in terms of polarization anisotropy of the optical properties were clearly observed and understood. In particular, methods for curing the native over-symmetry of classical envelope-function approach (EFA) have been proposed, following more or less explicitly the theory of invariants^{23,28–30}. These methods introduce at least one new interface parameter whose value is in general not provided within the same theory and must be fixed by comparison with experiment or more elaborate calculations, therefore their predictability is limited. From this point of view, NCA interfaces are particularly problematic, because specific interface bonds exist in a single direction, either (110) or $(\bar{1}10)$, and generally undergo considerable strain. For instance, in a InAs/AlSb quantum well, the host materials are nearly lattice matched, but nominal interfaces respectively involve In-Sb bonds that are 6.3% too long, and Al-As bonds that are 7.3% too short. Hence, one has to cope with very large, sharply localized strain, the modeling of which requires special attention. Finally, it is worth mentioning that desired or undesired atom exchange during growth can affect the composition of the interfacial layer, so that NCA QWs can exist with either nominal C_{2v} symmetry, or with same bonding at both

interfaces and D_{2d} symmetry, or in many intermediate, non-ideal configurations.

II. MODEL

Since atomic positions are an input of empirical tight-binding (ETB) models, the first problem to be solved is the relaxation of atomic positions under the effect of local interface strain. A zeroth order approach consists in extrapolating classical elasticity down to the single layer of chemical bonds, or molecular layer. Obviously, in order to go beyond this crude approximation, one must use atomistic elasticity such as the Valence Force Field (VFF) model^{31,32}. For sake of simplicity, we shall consider that the heterostructure is strained as a whole to maintain epitaxial relation to a GaSb substrate, but adaptation to the case of a “free-standing” superlattice is straightforward. In the classical elasticity limit the distance between atomic planes i and $i + 1$ is given, for each molecular layer, by $d_{i,i+1} = d_{i,i+1}^0 (1 + 2c_{12}/c_{11}(a_{i,i+1} - a_s)/a_s)$ where $a_{i,i+1}$ is the lattice parameter of the pseudo-binary compound corresponding to atomic planes i and $i + 1$ and a_s is the substrate parameter. c_{12} and c_{11} are the corresponding elastic constants. This result is obviously incorrect for an interface sequence like Sb=In-As since the In atom would have two highly strained “backward” bonds Sb=In, and two essentially unstrained “forward” bonds In-As.

Next we need to include equilibrium atomic positions and related strain effect in the extended-basis *spds** tight-binding formalism¹⁹. For bulk materials, it is widely accepted^{33,34} that, in addition to changes in phase factors and power-law scaling of two center transfer integrals with interatomic distances, one should consider that the on-site orbitals (in particular, the quasi-free electron orbitals d and s^*) feel the “geometry” of the deformed crystal, and their energies must therefore be shifted and possibly split according to the symmetry of the deformation. It was proved that this approach leads to satisfactory fit of bulk deformation potentials. Here we use a generalization of this scheme to the situation of an atom surrounded by arbitrarily chosen partners. Say we consider a cation C surrounded with 4 different anions A_i , $i = 1 - 4$, located at arbitrary positions, and need to define a local strain acting on the cation. Nominal Anion positions $\{\mathbf{r}_{0i}\}_{i=1..4}$ are first defined, using bond lengths corresponding to CA_i bulk lattice parameter and $[111]$ bond orientations. After relaxation, this nominal, unstrained tetrahedron transforms to the actual one with atoms at positions $\{\mathbf{r}_i\}_{i=1..4}$. The shapes of these tetrahedrons can be characterized using three arbitrarily chosen vectors $\{\mathbf{R}_j\}_{j=1..3}$. We choose them as: $\mathbf{R}_1 = \mathbf{r}_2 - \mathbf{r}_1$, $\mathbf{R}_2 = \mathbf{r}_4 - \mathbf{r}_3$, and $\mathbf{R}_3 = 1/2(\mathbf{r}_4 + \mathbf{r}_3 - \mathbf{r}_2 - \mathbf{r}_1)$. It is then easy to find the matrix T connecting the nominal and strained sets: $T\mathbf{R}_{0j} = \mathbf{R}_j$. The local strain tensor ϵ acting on on-site orbitals is defined by the polar decomposition $T = (1 + \epsilon)R$, where R is the orthogonal ma-

trix which rotates “nominal” tetrahedron to the strained one. One may notice that ϵ does not fully describe local atomic configuration: It is uniquely defined by the relative coordinates of four anions surrounding given cation (or vice versa) and the change of cation position does not affect local strain tensor. To account for the cation position we introduce additional internal strain vector \mathbf{u} defined as the (scaled to unstrained interatomic distance) displacement of cation from the centre of sphere which touches surrounding anions. Note that in a bulk material, strain and internal displacement are proportional and related by the Kleinman parameter ζ , which is not the case for atomic positions in a situation of arbitrary chemical surrounding. As done implicitly in Ref. 33, we assume that the effect of the internal strain on tight-binding Hamiltonian is the same as that of the strain tensor part which transforms as a vector. In summary, the local strain hamiltonian acting on p orbitals (p_x, p_y, p_z) and d orbitals with the symmetry Γ_{15} (d_{yz}, d_{zx}, d_{xy}) on-site orbitals is written as:

$$\delta\hat{H} = \begin{pmatrix} \lambda_1(\sqrt{3}\epsilon_1 - \epsilon_2) & \lambda_2(\epsilon_{xy} + \xi u_z) & \lambda_2(\epsilon_{zx} + \xi u_y) \\ \lambda_2(\epsilon_{xy} + \xi u_z) & -\lambda_1(\sqrt{3}\epsilon_1 + \epsilon_2) & \lambda_2(\epsilon_{yz} + \xi u_x) \\ \lambda_2(\epsilon_{zx} + \xi u_y) & \lambda_2(\epsilon_{yz} + \xi u_x) & 2\lambda_1\epsilon_2 \end{pmatrix}$$

where we use $\epsilon_1 = \sqrt{3}(\epsilon_{xx} - \epsilon_{yy})$, $\epsilon_2 = 2\epsilon_{zz} - \epsilon_{xx} - \epsilon_{yy}$. In notation of Ref. 33, for p -orbitals $\lambda_1 = \frac{1}{2}E_p\pi_{001}$, $\lambda_2 = \frac{8}{3}E_p\pi_{111}$ and for d -orbitals $\lambda_1 = \frac{1}{2}E_d\delta_{001}$, $\lambda_2 = \frac{8}{3}E_d\delta_{111}$. The parameter ξ is equal to +1 for cations and to -1 for anions. Note that in principle, π and δ parameters may have different values for anions and cations. These prescriptions give the same result as in Ref. 33 for strained bulk semiconductors.

However, an obvious difficulty with this general frame is the large number of parameters that need to be determined: it is clear that the sole consideration of deformation potentials at the zone center (that are reasonably well documented) does not provide enough information. On the other hand, even the most sophisticated ab initio schemes still encounter difficulties with conduction band dispersions, and blind fitting may lead to unsatisfactory parameterization. For the present purpose, one can rely on any parameterization that gives sound values of a_c, v , b and d . Here, we reworked the strain parameters using an optimization algorithm and looking for a set of strain parameters close to the one of Ref. 19 and that reproduces the recommended values of deformation potentials in the center of Brillouin zone given in Ref. 35. For simplicity, since π and δ parameters have the same effects on deformation potentials in Γ point, δ parameters were set to zero and thus renormalised in π parameters. Strain parameters used in present calculations and resulting zone-center deformation potentials are listed in tables I and II.

TABLE I. Strain parameters used in calculations, and resulting zone-center deformation potentials. Notations from Ref. 33

	AlAs	InAs	AlSb	InSb
n_s	0.6665	0.7300	1.0570	0.4390
n_p	0.9626	1.6282	1.8518	1.7595
n_d	1.7296	1.6756	1.9764	1.8372
n_{s^*}	2.0000	2.0000	2.0000	2.0000
$n_{ss\sigma}$	2.1300	2.7400	2.7980	4.7900
$n_{sp\sigma}$	3.8720	2.9100	3.3320	3.8540
$n_{sd\sigma}$	2.1740	1.4860	2.1760	1.7060
$n_{ss^*\sigma}$	0.0000	0.0000	0.0000	0.0000
$n_{s^*s^*\sigma}$	0.0000	0.0000	0.0000	0.0000
$n_{s^*p\sigma}$	1.9200	1.1060	1.3360	1.3540
$n_{s^*d\sigma}$	2.0000	2.0000	2.0000	2.0000
$n_{pp\sigma}$	2.7720	2.7180	2.9080	1.8360
$n_{pp\pi}$	4.3580	4.8720	3.4060	4.3100
$n_{pd\sigma}$	2.3330	2.6650	2.6710	2.0050
$n_{pd\pi}$	2.4729	1.3749	0.8629	2.0769
$n_{dd\sigma}$	2.6120	1.3780	1.1780	2.9980
$n_{dd\pi}$	1.7320	2.7980	2.9540	2.9580
$n_{dd\delta}$	2.8720	1.0000	1.6800	1.0160
π_{001}	0.1530	0.1610	0.2970	0.3000
π_{111}	0.3540	0.4910	0.6020	0.3350
δ_{001}	0.0000	0.0000	0.0000	0.0000
δ_{111}	0.0000	0.0000	0.0000	0.0000

TABLE II. Tight-binding deformation potentials of bulk materials. The fitted values are identical to the target values taken from Ref 35, except that we use the sign convention for a_v , such that bandgap is proportional to $a_c - a_v$.

	AlAs	InAs	AlSb	InSb
a_c	-5.64	-5.08	-4.50	-6.94
a_v	2.47	1.00	1.40	0.36
b	-2.30	-1.80	-1.35	-2.00
d	-3.40	-3.60	-4.30	-4.70

III. RESULTS AND DISCUSSIONS

The approach outlined in previous section is similar to that introduced by C. Pryor³⁶ and used by R. Magri et al. for the AEPP approach^{37,38}, or to that used by M. Zielinski for EPTB³⁴. It differs however on a very important item that is the unambiguous definition of the internal displacement vector that is mandatory for proper account of trigonal deformations³³. Yet, to the best of our knowledge, these atomistic models were not validated by a crucial comparison with a well-established experimental result. A possible test case is an In monolayer inserted in a GaAs matrix. The experimental gap is well documented with a low temperature value of 1.434 eV from optical properties of samples containing a slightly sub-monolayer amount of In giving raise to large, monolayer thick islands³⁹. Our calculations give a value of 1.436 eV when using a “natural valence band offset” (VBO) of 0.23 eV, which is consistent with experimental VBO value for $\text{In}_{0.15}\text{Ga}_{0.85}\text{As}/\text{GaAs}$ superlattices⁴⁰. Note that

TABLE III. Interplane distances in the vicinity of interfaces. VFF calculations are made for a several period 8/8 InAs/AlSb superlattice grown on a GaSb substrate.

	h bulk	h classical	h VFF
Al-Sb	1,5339	1.5437	1.5436
Sb=Al	1,5339	1.5437	1.5441
Al-Sb	1,5339	1.5437	1.5367
Sb=In	1,6198	1.7234	1.7323
In-As	1,5146	1.5041	1.4962
As=In	1,5146	1.5041	1.5046
In-As	1,5146	1.5041	1.5041
In-As	1,5146	1.5041	1.5041
As=In	1,5146	1.5041	1.5035
In-As	1,5146	1.5041	1.5132
As=Al	1,4150	1.3219	1.2958
Al-Sb	1,5339	1.5437	1.5541
Sb=Al	1,5339	1.5437	1.5428
Al-Sb	1,5339	1.5437	1.5436

including the piezoelectric potential into the calculation reduces the gap by 4 meV.

Next we come to InAs/AlSb superlattices. In Table III, we compare the atomic distances in the interface regions of a 8/8 InAs/AlSb superlattice, obtained in the “classical” and “atomistic” elasticity models. For the latter, we use the Keating parameters of Ref. 31. It can be observed that in the VFF calculations, interface strain perturbs the atomic positions on typically one monolayer (3Å) on both sides of the “anomalous” interface bond, with an oscillatory behavior before the interplane distances stabilize to the classical elasticity value. Somewhat counter-intuitively, the deformation of anomalous interface bonds along the growth axis is larger (typically 10%) in the VFF calculation, compared to classical elasticity.

In table IV, we show the local strain tensor associated with the different atomic sites in a 8/8 InAs/AlSb superlattice, using the VFF atomic positions. A remarkable, perhaps counterintuitive feature is the existence of a trigonal (shear) component ϵ_{xy} for atoms that have an asymmetrical chemical surrounding.

The bulk material parameters used in this work are listed in Table V. The calculation also requires band offset values. For the well-documented offsets for the nearly unstrained heteropairs InAs/GaSb, InAs/AlSb and GaSb/AlSb we take respectively 570, 200 and 350 meV. Experimental values agree with ab initio calculations. Unfortunately, the situation for InSb/InAs is not as clear, with no direct experimental result and a strong dispersion of theoretical predictions from 400 meV⁴¹ to 700 meV⁴².

The molecular layer of InSb certainly act as a “potential well” in the valence band, but uncertainty in VBO implies that the depth of this trap is unknown, and we shall consider it as the only free parameter in the calculations. Conversely, the AlAs bonds act as a “potential barrier” whose height is also not so well documented, but the impact of this uncertainty on our results is actually

TABLE IV. local strain tensor acting on atomic orbitals on-site energies for a 8/8 InAs/AlSb superlattice grown lattice-matched to a GaSb substrate.

	$\epsilon_{xx}(\%)$	$\epsilon_{yy}(\%)$	$\epsilon_{zz}(\%)$	$\epsilon_{yz}(\%)$	$\epsilon_{zx}(\%)$	$\epsilon_{xy}(\%)$	$u_z(\%)$
In	-2.647	-2.647	3.005	0.	0.	3.272	4.349
As	0.626	0.626	-0.930	0.	0.	0.	-0.160
In	0.626	0.626	-0.669	0.	0.	0.	0.010
As	0.626	0.626	-0.686	0.	0.	0.	-0.001
In	0.626	0.626	-0.685	0.	0.	0.	0.
As	0.626	0.626	-0.685	0.	0.	0.	0.
In	0.626	0.626	-0.685	0.	0.	0.	0.
As	0.626	0.626	-0.685	0.	0.	0.	0.
In	0.626	0.626	-0.685	0.	0.	0.	0.
As	0.626	0.626	-0.685	0.	0.	0.	0.
In	0.626	0.626	-0.685	0.	0.	0.	0.
As	0.626	0.626	-0.685	0.	0.	0.	0.
In	0.626	0.626	-0.685	0.	0.	0.	0.
As	0.626	0.626	-0.685	0.	0.	0.	0.
In	0.626	0.626	-0.684	0.	0.	0.	-0.001
As	0.626	0.626	-0.703	0.	0.	0.	0.012
In	0.626	0.626	-0.403	0.	0.	0.	-0.189
As	4.163	4.163	-4.112	0.	0.	-3.538	4.399
Al	3.528	3.528	-3.358	0.	0.	-4.173	-5.170
Sb	-0.645	-0.645	0.950	0.	0.	0.	0.216
Al	-0.645	-0.645	0.611	0.	0.	0.	-0.016
Sb	-0.645	-0.645	0.636	0.	0.	0.	0.001
Al	-0.645	-0.645	0.635	0.	0.	0.	0.
Sb	-0.645	-0.645	0.635	0.	0.	0.	0.
Al	-0.645	-0.645	0.635	0.	0.	0.	0.
Sb	-0.645	-0.645	0.635	0.	0.	0.	0.
Al	-0.645	-0.645	0.635	0.	0.	0.	0.
Sb	-0.645	-0.645	0.635	0.	0.	0.	0.
Al	-0.645	-0.645	0.635	0.	0.	0.	0.
Sb	-0.645	-0.645	0.635	0.	0.	0.	0.
Al	-0.645	-0.645	0.634	0.	0.	0.	0.001
Sb	-0.645	-0.645	0.650	0.	0.	0.	-0.010
Al	-0.645	-0.645	0.427	0.	0.	0.	0.139
Sb	-3.282	-3.282	3.657	0.	0.	2.637	-3.580

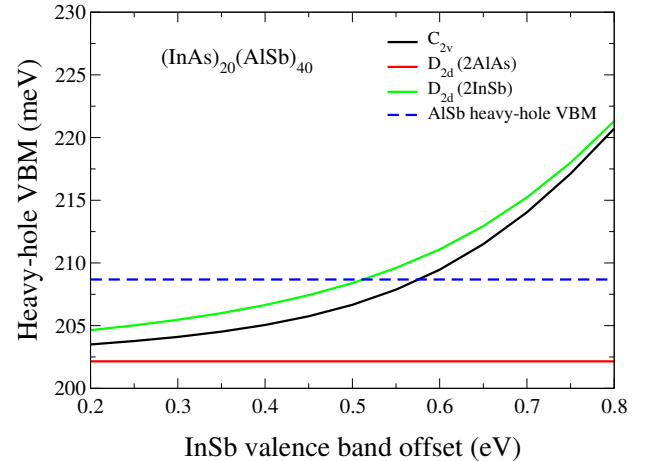


FIG. 2. Heavy-hole ground state energy for a 20/40 InAs/AlSb superlattice for C_{2v} , D_{2d} , 2AlAs and D_{2d} , 2 InSb interface configurations. The origin of energies is the unstrained InAs valence band maximum (VBM). The AlSb heavy-hole VBM is shown as the horizontal line at 208.7 meV.

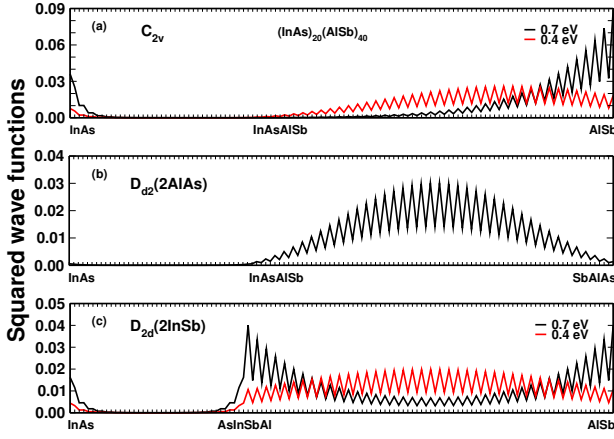


FIG. 3. a) Heavy hole ground state wave function for a 20/40 InAs/AlSb SL, for two values of the InSb band offset, 700 and 400 meV. A solid line is drawn to connect tight binding on-site amplitudes for clarity. In all these materials, valence band eigenstates have a strongly dominant Anion character; b, c) Same for the D_{2d} , 2 AlAs and D_{2d} , 2 InSb configurations.

negligible. When epitaxial strain is taken into account, the AlSb heavy-hole band extremum lies at 208.7 meV above the arbitrary reference level of unstrained InAs VBM. The heavy hole confinement in a regular 12.2 nm-thick (40 monolayers) QW is 6.4 meV. Hence, one reasonably expects a hole ground state at 202.3 meV. Fig. 2 shows the evolution of actual hole ground state energy in a 20/40 InAs/AlSb superlattice as a function of InSb band offset, for the 3 ideal situations: “ C_{2v} ” (AlAs and InSb interfaces), “ D_{2d} ” (2 AlAs) and “ D_{2d} ” (2 InSb). In C_{2v} case for InAs/InSb VBO larger than 600 meV, the ground state is above the AlSb VBM, hence it is clearly trapped by the InSb bond. For smaller offsets, the ground state lies between the AlSb VBM and 204 meV: the situation is better described as a regular quantum well with an attractive perturbation at one interface, that decreases the confinement energy and polarizes the wavefunction. As shown in Fig. 3a, in all cases the wavefunction is strongly asymmetrical with respect to the center of AlSb layer: As long as AlSb thickness remains finite, it is difficult to define a rigorous criterium for existence of an interface state. By exploring numerically larger layer thicknesses, we find that 500 meV is a practical threshold offset value for the existence of an interface state at a InSb interface between InAs and AlSb.

The D_{2d} case with two AlAs interfaces (see Figs. 2, 3b) corresponds to the regular quantum well case. The D_{2d} 2 InSb configuration is more interesting, because interface states may exist at both interfaces, and combine into symmetric (bonding) or antisymmetric (antibonding) states, with a splitting depending strongly on AlSb layer thickness. Due to this interaction, the ground state energy remains nearly constant when decreasing the AlSb thickness. This result is illustrated in Fig. 4. A similar trend is also valid for interface state coupling through the InAs layer, but to a much smaller extent due to the

TABLE V. Tight-binding parameters used in calculations.

	InAs	InSb	AlAs	AlSb
a	6.0580	6.4794	5.6600	6.1355
E_s^a	-6.4738	-6.1516	-5.9874	-6.0025
E_s^{a*}	16.8502	14.7582	19.5074	16.4623
E_s^c	-0.1418	-0.3634	0.9483	0.6705
E_s^{c*}	16.8393	14.8015	19.5038	16.4797
E_p^a	2.4784	2.1150	3.4914	2.5476
E_d^a	11.3833	9.8811	13.0560	11.1777
E_p^c	5.2829	5.5198	6.3335	5.8536
E_d^c	11.3991	9.9511	13.0592	11.1500
$ss\sigma$	-1.5096	-1.2228	-1.8436	-1.4804
$s_a s_c^* \sigma$	-2.0155	-1.6619	-1.7884	-2.9492
$s_a^* s_c \sigma$	-1.1496	-1.3929	-1.3059	-1.4096
$s^* s^* \sigma$	-3.3608	-2.8985	-3.6128	-1.2369
$s_a p_c \sigma$	2.2807	2.2046	2.5778	2.2550
$s_c p_a \sigma$	2.6040	2.3639	2.7962	2.5961
$s_a^* p_c \sigma$	1.9930	1.6962	2.1581	2.1314
$s_c^* p_a \sigma$	2.0708	1.9879	2.2397	1.9456
$s_a d_c \sigma$	-2.8945	-2.3737	-2.5623	-2.5320
$s_c d_a \sigma$	-2.3175	-2.1766	-2.3841	-2.0483
$s_a^* d_c \sigma$	-0.6393	-0.5548	-0.8045	-0.5304
$s_c^* d_a \sigma$	-0.5949	-0.4875	-0.7491	-0.5989
$pp\sigma$	3.6327	3.4603	4.1970	3.7007
$pp\pi$	-0.9522	-1.1630	-1.3145	-1.2989
$p_a d_c \sigma$	-1.1156	-1.3928	-1.6473	-1.3211
$p_c d_a \sigma$	-1.3426	-1.4145	-1.7603	-1.7320
$p_a d_c \pi$	1.2101	1.1921	1.7646	1.6944
$p_c d_a \pi$	1.5282	1.7536	2.1099	1.7783
$dd\sigma$	-0.8381	-0.6688	-1.2241	-0.9481
$dd\pi$	1.9105	1.4601	2.1770	1.8128
$dd\delta$	-1.3348	-1.4373	-1.7585	-1.6148
$\Delta_a/3$	0.1558	0.3810	0.1721	0.3454
$\Delta_c/3$	0.1143	0.1275	0.0072	0.0121

fast decay of interface state into InAs. Note however that his remark holds only in as much as the unavoidable difference between the two interface state energies is smaller than their mutual coupling. Results displayed in Fig. 3 are qualitatively similar to those obtained from LDA calculations by Shaw et al.¹⁰, but the decay of interface state in AlSb is much slower in our calculations. It is noteworthy that calculations of Ref. 10 do not include spin-orbit interaction and therefore, the effective valence band quantum wells differ. Finally, it is interesting to examine the effect of a change in InAs/AlSb VBO, within the experimental uncertainty range 150 ± 50 meV: the smaller this offset is, the easier it is for the interface trap to capture the valence ground state. For vanishing InAs/AlSb VBO, any value of InSb VBO would lead to an interface state, whose decay in both layers would become almost symmetrical. In Fig 5, we show the dependencies on InSb/InAs offset for a InAs/AlSb offset of 100 meV. It is seen that in this case, the interface state exists as soon as the InSb/InAs offset exceeds 314 meV.

So far, we have discussed interface potential in terms of a “diagonal” or scalar contribution. However, as mentioned in the introduction, interface also break a rotational invariance and corresponding Hamiltonian ad-

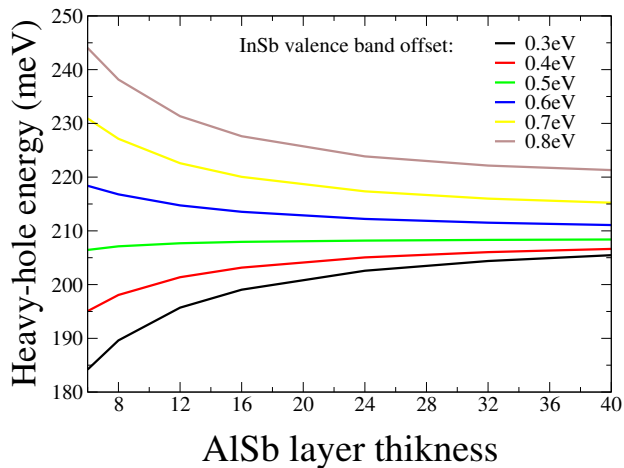


FIG. 4. Dependence of heavy-hole ground state energy on AlSb layer thickness for the D_{2d} , 2 InSb configuration.

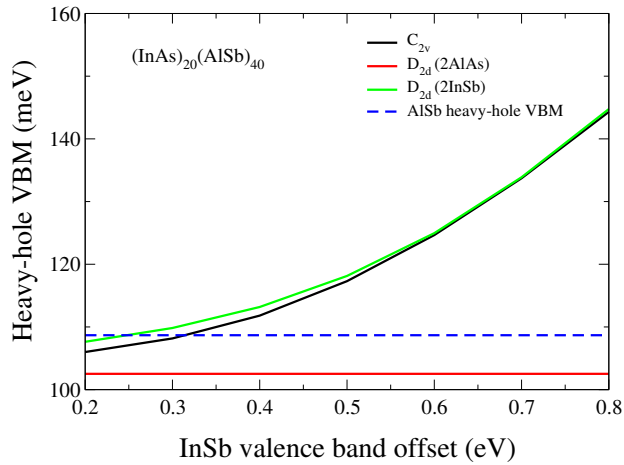


FIG. 5. Analogous to Fig 2 with InAs/AlSb VBO = 100 meV.

mixes heavy and light holes, which results in the linear polarization of optical spectra when system has C_{2v} symmetry^{22,28,30}. Here, valence states are confined in the AlSb layer, and ground state peaks close to the InSb bonds. They undergo the strong spin-orbit coupling of Sb. Since spin-orbit interaction tends to force total angular momentum eigenstates, weak polarization anisotropy is expected. This anisotropy is confirmed by the calculations: For the 20/40 InAs/AlSb superlattice, we obtain a degree of linear polarization of the ground optical transition (with principal axis along the $[1,1,0]$ and $[-1,1,0]$ directions) equal to 6%.

IV. CONCLUSION

We have used extended-basis tight-binding to model the no-common atom system of InAs/AlSb with the highest possible accuracy. We find that for a large range of the natural band offset of InSb, there exists an intrinsic interface state “trapped” by the plane of interfacial InSb bonds. The existence of such a state is important for valence band physics in this system, but also plays an important role in the material characterization using interband optics.

V. ACKNOWLEDGEMENTS

The authors thank Dr. F. Glas for fruitful discussions and for cross-checking VFF atomic positions. This work was supported in part by ANR “SNAP”, by French-Russian Int. Laboratory “ILNACS”, and by “Triangle de la Physique CAAS”.

- ¹ I. E. Tamm, Zh. Eksp. Teor. Fiz. **3**, 34 (1933).
- ² M. Z. Hasan and C. L. Kane, Rev. Mod. Phys. **82**, 3045 (2010).
- ³ G. Bastard, Phys. Rev. B **25**, 7584 (1982).
- ⁴ Y.-C. Chang, J. N. Schulman, G. Bastard, Y. Guldner, and M. Voos, Phys. Rev. B **31**, 2557 (1985).
- ⁵ J. N. Schulman and Y.-C. Chang, Phys. Rev. B **33**, 2594 (1986).
- ⁶ G. Bastard, Phys. Rev. B **24**, 5693 (1981).
- ⁷ G. Bastard, *Wave Mechanics Applied to Semiconductors Heterostructures* (Les Editions de Physique, Paris, 1988).
- ⁸ H. Kroemer, C. Nguyen, and B. Brar, Journal of Vacuum Science & Technology B **10**, 1769 (1992).
- ⁹ R. G. Dandrea and C. B. Duke, Applied Physics Letters **63**, 1795 (1993).
- ¹⁰ M. J. Shaw, P. R. Briddon, and M. Jaros, Phys. Rev. B **52**, 16341 (1995).
- ¹¹ M. J. Shaw, Phys. Rev. B **58**, 7834 (1998).
- ¹² Y.-S. Kim, M. Marsman, G. Kresse, F. Tran, and P. Blaha, Phys. Rev. B **82**, 205212 (2010).

- ¹³ I. Vurgaftman, J. R. Meyer, and L. R. Ram-Mohan, Journal of Applied Physics **89** (2001).
- ¹⁴ H. Kroemer, Rev. Mod. Phys. **73**, 783 (2001).
- ¹⁵ R. Teissier, D. Barate, A. Vicet, C. Alibert, A. N. Baranov, X. Marcadet, C. Renard, M. Garcia, C. Sirtori, D. Revin, and J. Cockburn, Applied Physics Letters **85**, 167 (2004).
- ¹⁶ J. Nicolai, C. Gatel, B. Warot-Fonrose, R. Teissier, A. N. Baranov, C. Magen, and A. Ponchet, Applied Physics Letters **104**, 031907 (2014).
- ¹⁷ C. Colliex, Journal of Electron Microscopy **60**, S161 (2011).
- ¹⁸ B. Fain, I. Robert-Philip, A. Beveratos, C. David, Z. Z. Wang, I. Sagnes, and J. C. Girard, Phys. Rev. Lett. **108**, 126808 (2012).
- ¹⁹ J.-M. Jancu, R. Scholz, F. Beltram, and F. Bassani, Phys. Rev. B **57**, 6493 (1998).
- ²⁰ A. Zunger, *Quantum Theory of Real Materials* (edited by J. R. Chelikowsky and S. G. Louie (Kluwer, Boston, 1996), 1996).

- ²¹ G. Bester, *Journal of Physics: Condensed Matter* **21**, 023202 (2009).
- ²² G. Theodorou and G. Tsegas, *Phys. Rev. B* **61**, 10782 (2000).
- ²³ E. L. Ivchenko and M. O. Nestoklon, *Phys. Rev. B* **70**, 235332 (2004).
- ²⁴ J. N. Schulman and Y.-C. Chang, *Phys. Rev. B* **24**, 4445 (1981).
- ²⁵ J. N. Schulman and Y.-C. Chang, *Phys. Rev. B* **27**, 2346 (1983).
- ²⁶ Y.-C. Chang and J. N. Schulman, *Phys. Rev. B* **31**, 2069 (1985).
- ²⁷ D. L. Smith and C. Mailhot, *Rev. Mod. Phys.* **62**, 173 (1990).
- ²⁸ O. Krebs and P. Voisin, *Phys. Rev. Lett.* **77**, 1829 (1996).
- ²⁹ I. L. Aleiner and E. Ivchenko, *JETP* **55**, 692 (1992).
- ³⁰ E. Ivchenko, A. Toropov, and P. Voisin, *Physics of the Solid State* **40**, 1748 (1998).
- ³¹ P. N. Keating, *Phys. Rev.* **145**, 637 (1966).
- ³² R. M. Martin, *Phys. Rev. B* **1**, 4005 (1970).
- ³³ J.-M. Jancu and P. Voisin, *Phys. Rev. B* **76**, 115202 (2007).
- ³⁴ M. Zieliński, *Phys. Rev. B* **86**, 115424 (2012).
- ³⁵ I. Vurgaftman, J. R. Meyer, and L. R. Ram-Mohan, *Journal of Applied Physics* **89** (2001).
- ³⁶ C. Pryor, J. Kim, L. W. Wang, A. J. Williamson, and A. Zunger, *Journal of Applied Physics* **83**, 2548 (1998).
- ³⁷ R. Magri and A. Zunger, *Phys. Rev. B* **64**, 081305 (2001).
- ³⁸ P. Piquini, A. Zunger, and R. Magri, *Phys. Rev. B* **77**, 115314 (2008).
- ³⁹ O. Brandt, L. Tapfer, R. Cingolani, K. Ploog, M. Hohenstein, and F. Phillipp, *Phys. Rev. B* **41**, 12599 (1990).
- ⁴⁰ B. Soucail, N. Dupuis, R. Ferreira, P. Voisin, A. P. Roth, D. Morris, K. Gibb, and C. Lacelle, *Phys. Rev. B* **41**, 8568 (1990).
- ⁴¹ S. Wei and A. Zunger, *Journal of Vacuum Science & Technology B* **5**, 1239 (1987).
- ⁴² Van de Walle Chris G. and Neugebauer J., *Nature* **423**, 626628 (2003).